Energy & Buildings 263 (2022) 112044

Contents lists available at ScienceDirect

Energy & Buildings

journal homepage: www.elsevier.com/locate/enb

Thermal response time prediction-based control strategy for radiant floor heating system based on Gaussian process regression

Qiong Chen, Nan Li *

National Centre for International Research of Low-carbon and Green Buildings, Ministry of Science & Technology, Chongqing University, Chongqing 400045, China

ARTICLE INFO

Article history:
Received 14 January 2022
Revised 8 March 2022
Accepted 21 March 2022
Available online 23 March 2022

Keywords:
Control strategy optimization
Response time prediction
Gaussian process regression
Radiant floor system
Sensitivity analysis

ABSTRACT

One of the main obstacles to wider applications of radiant floor heating systems with great thermal comfort and energy efficiency is the long response time caused by large thermal inertia and little research has been conducted to effectively address this issue. In this study, an optimal control strategy based on a thermal response time prediction model for radiant floor heating systems was proposed by applying the gaussian process regression (GPR) algorithm. First, a comprehensive database of the thermal response time for various scenarios based on different building configurations, radiant floor, and weather characteristics was obtained by parametric simulations after base-case building validation. Then a sensitivity analysis of the response performance of the seven explanatory variables by Pearson correlation coefficients was conducted and a theoretical explanation was provided. Besides, the response time prediction model based on the GPR algorithm with a larger R^2 of around 0.96 was obtained by an in-depth comparison with commonly used machine learning algorithms such as multiple linear regression, random forest, and support vector machines. Its accuracy was verified by cross-validation and a 25% database. Finally, an optimal control strategy based on the response time prediction model was proposed which can reduce the response time from 96 ~ 188 mins to 44 ~ 75 mins, achieving a reduction of 41% ~ 64% while keeping the comparative power consumption. Therefore, the proposed optimal control strategy can effectively reduce the thermal response time of radiant floor heating systems and improve the indoor thermal comfort during the thermal response phase without sacrificing power consumption.

1. Introduction

Space heating areas of residential buildings rose to 814399.26 million square meters while accounting for about 74% of the total heating areas of China in 2019 according to China Urban-Rural Construction Statistical Yearbook 2019 [1]. Better thermal comfort and great potential of energy-saving enable the widespread application of radiant heating and cooling systems in residential buildings as an alternative to conventional HVAC systems [2,3]. State-of-the-art control strategies which have been demonstrated to be beneficial to the optimal operation for a variety of space heating systems are encouraged to be implemented into practice for exploiting the energy-saving potential of radiation systems [4,5].

The control methods and strategies applied to the radiant heating and cooling systems [6] mainly include the bang-bang control [7], water temperature control, water flow control [8]. Bang-bang control refers to the switch control where the preset control will be activated when the target variable is above the upper limit or below the lower limit of the control interval. There is no control action while the control target is within the range of the control interval. The bang-bang control can be easily put into implementation as the most simplified and feasible control method [9]. The only two states of start or stop of the bang-bang control are on operation when the thermal zones are occupied or not usually [10,11]. However, its applicable implementation on radiant heating and cooling systems has been hindered by the larger thermal inertia compared with conventional space heating systems [12]. The intense zone air temperature overshoot and lower control flexibility have demonstrated the poor dynamic performance and energy efficiency of the bang-bang control's application on radiant heating and cooling systems [13].

Water temperature control is an open-loop or closed-loop control system that uses water temperature as the controlled variable [14]. It is a way to regulate the heat supply from the HVAC system to the thermal zones by controlling the variable water temperature to accommodate fluctuations of the building heat load caused by the outdoor environment changes [15]. Keeping a constant water flow rate ensures a stable hydraulic network balance and brings

* Corresponding author.
E-mail address: nanlicqu@163.com (N. Li).

https://doi.org/10.1016/j.enbuild.2022.112044
0378-7788/

Nomenclature

T_{resp}	Response time of radiant floors, second.
$Q_{heatload}$	Heat load of radiant floors, W/m^2.
Q_{supply}	Heat supply of radiant floors, W/m^2.
T_{amb}	Ambient temperature, °C.
$T_{z,set}$	Zone air temperature setpoint, °C.
Q_{equip}	Heat gain from internal equipment, W/m^2.
$Q_{infiltration}$	Heat gain from infiltration loss, W/m^2.
Q_{solar}	Heat gain from solar radiation, W/m^2.
T_{ws}	Water supply temperature, °C.
ϑ_w	Water velocity in buried pipe of radiant floors, m/s.
d_o	Pipe diameter of buried pipe of radiant floors, m.
d_x	Pipe spacing of radiant floors, m.
d_{filler}	Filler course thickness of radiant floors, m.
T_{zi}	Initial zone air temperature, °C.
S/V	Shape factor.
R^2	Determination coefficient.
Q_p	Power consumption of the air-source heat pump, kWh.
Q_h	Heat supply of the air-source heat pump, kWh.
COP	Coefficient of performance of the air-source heat pump.

Abbreviations

GPR	Gaussian process regression.
ML	Machine learning.
MLR	Multiple linear regression.
RF	Random forest.
SVM	Support vector machine.
GP	Gaussian process.
MBE	Mean bias error.
CV(RMSE)	Coefficient of variation of the root mean square error.
MAE	Mean absolute error.
MSE	Mean squared error.
RMSE	Root mean square error.
GA	Genetic algorithm.
ANN	Artificial neural network.

the advantages of simple management and easy operation [16]. However, it also leads to higher power consumption while large public buildings or centralized heating systems use only water temperature control. The water temperature control system will encounter a series of problems such as poor system stability, the high frequency of adjustment action, and the large static difference [17]. The system greatly influenced by the ambient environment cannot achieve complex control algorithms [18]. Besides, water temperature control has typical hysteresis characteristics that many factors contribute to [19].

Water flow control is a regulation method that maintains the designed water supply temperature throughout the heating period and constantly changes the water flow rate at the heat source as the time-varying ambient temperature to accommodate the variable heat load [20,21]. This type of control method for heating and cooling systems adopts the exact different control variable compared with the water temperature control while sharing the opposite advantages and disadvantages of the control performance [22]. The rapidly decreasing water flow rate often causes serious non-homogeneous heat distribution in multi-zone heating systems as the outdoor temperature rises [23,24]. At the same time, constantly changing the water flow rate of the network as the ambient temperature changes demand a more complex system configuration [25] and often requires variable speed pumps to achieve flow regulation in practice operation.

In addition to the above conventional control methods [2], the prevalence of intelligent technology has given rise to many smart control methods applicable to the building industry for energy efficiency improvement [26], better indoor thermal comfort [27], enhanced indoor pollutant concentration control, etc. [28] Jingjuan (Dove) Feng et al. [4] developed and calibrated the simplified dynamic heat transfer model for the radiant slab system and a real-time MPC (model predictive control) was further was established for the built building model. Compared with the rule-based control strategy, the real-time MPC can achieve a 55% reduction in cooling tower consumption and a 25% reduction in water pump consumption while maintaining the zone operative temperature at the EN 15251 Category II level for 95% occupied duration. Xiufeng Pang et al. [29] proposed the simplified MPC toolchain for better implementation in the building industry by eliminating the main barriers of the high computational cost and challenging complexity after validating the effectiveness of the developed MPC with experimental measurements. The established MPC was applied to the radiant slab system in the FLEXLAB building test facility at the Lawrence Berkeley National Laboratory and achieved 42% of water pump power reduction and 16% of energy consumption saving compared with the heuristic control strategy.

Jaewan Joe et al. [30] developed a parametric identification-based modeling approach for diverse thermal comfort requirements in multiple zones. This inverse modeling approach enhanced the scalability and flexibility of the building model by integrating individual sub-building models, and then the accuracy of the modeling approach was validated with actual operational data. The experimental results showed that the established distributed MPC reduced the electricity consumption of the radiant floor cooling system by 27% relative to the feedback control and achieved diverse thermal comfort for different office areas at the same time. Besides, they implemented the proposed MPC into the practice operation of the radiant floor system which can minimize the energy consumption and running cost according to the outdoor weather and building load prediction [31]. The field implementation yielded 34% of running cost savings and 16% of energy consumption reduction for the cooling and heating seasons compared with the feedback control, respectively. Dongliang Zhang et al. [32] developed the state-of-the-art MPC for the radiant ceiling cooling integrated with an underfloor ventilation system and reduced energy consumption by 13.2% compared with PID control in the field implementations. Furthermore, the MPC proposed by them yielded 17.5% energy saving compared with the PID control for the radiant floor cooling combined with an underfloor ventilation system while maintaining comparative or better thermal comfort [33].

Martin Schmelas et al. [18] proposed an adaptive and predictive control for the thermo-active building systems based on the multiple regression algorithm, which can achieve better thermal comfort and load shift after validation by the experimental measurements. Then this proposed control approach was put into practice for performance evaluation of the energy-saving and thermal comfort improvement, and more than 41% of energy savings and 95% of the occupied time of the comfort norms ISO7730 and DIN EN 15251 were demonstrated by experiment results [34]. Furthermore, this novel adaptive and predictive control method was applied to the operation of a passive seminar building for about nine months along with the conventional control strategy for the thermo-active building systems. The operation results showed that the running time of the water pump was reduced largely and the energy-saving up to 26% was obtained while maintaining a better thermal comfort [19].

Georgios Lymperopoulos and Petros Ioannou [35] proposed a distributed adaptive control approach for the zone air temperature regulation of the multi-zone building HVAC systems by employing online learning technology. The dynamic performance of this control method was evaluated in a six-zone building and a primary school building in EnergyPlus. The simulation results showed that the introduction of adaptive learning brought more accurate zone air temperature control and energy efficiency benefits. Yuebo Meng et al. [36] proposed an occupancy-based predictive control method by applying the deep learning image detection technology, by which the occupancy heat load was available by estimating the real-time occupants' numbers. The simulation results of a student activity center and a small-scale office building confirmed the improved performance on the environmental comfort and faster system response.

To address the problem of high accuracy on building models and cost-ineffective sensor installation, Shunian Qiu et al. [37] developed a model-free optimal control method for a building cooling water system based on reinforcement learning. The simulations results indicated that the lower energy efficiency of the model-free control method was caused by the insufficient learning of fewer than three months while it can still provide promising application prospects. Dasheng Lee et al. [21] developed a smart-valve-assisted model-free predictive control for no data available situation for the chiller plants based on reinforcing learning. The experimental measurements of a hospital, an office building, and a factory demonstrated the 30% reduction in energy consumption and the prompt scalability compared with other massive data-based intelligent control technology.

In summary, MPC has been increasingly applied in the conventional space heating and cooling systems, thermo-active or radiant building systems in a lot of previous research while the high computational cost and cost-ineffective implementation have always been the obstacles that hindered the widespread application in the actual buildings, particularly in residential buildings due to the complicated installation and high initial cost for users [38,39]. Furthermore, the control performance of other model-based adaptive control methods is highly dependent on the model accuracy and adequate sensors, which are principally difficult to access in residential buildings [40]. Despite research efforts placed on advanced control methods [41], few studies have been oriented from the thermal response time performance perspective, whereas the longer thermal response time performance is the main obstacle hindering the efficient operation of radiant floor heating systems compared to conventional spacing heating systems. The prediction model of the thermal response time of radiant floor heating system is supposed to be developed to solve the problem of long thermal response time and indoor thermal comfort performance degradation, while the previous researches focus on the building energy prediction model.

In this study, an optimal control strategy based on a thermal response time prediction model for radiant floor heating systems is proposed and evaluated as shown in Fig. 1. First, a base case building model is developed by TNRSYS and validated by experimental results. Then, parametric simulations based on various building characteristics, radiant floor features, and weather information are conducted to obtain a comprehensive database of thermal response performance for all these cases. In addition, a sensitivity analysis of the response performance to all those explanatory variables is performed by Pearson correlation coefficients, and a comprehensive theoretical interpretation of the sensitivity analysis results is presented. After that, the response time prediction model of radiant floor heating system based on GPR algorithm is obtained by an extensive comparison of commonly used machine learning (ML) algorithms such as multiple linear regression (MLR), random forest (RF), and support vector machine (SVM). And its accuracy is verified by cross-validation and 25% database collection. Finally, an optimal control strategy based on the response time prediction model is proposed and compared with the conventional intermittent operation strategy in terms of response performance and energy efficiency.

2. Base case calibration and parametric simulation

2.1. Base case calibration

The residential building equipped with a radiant floor heating system located in Chongqing, China was selected as the base case,

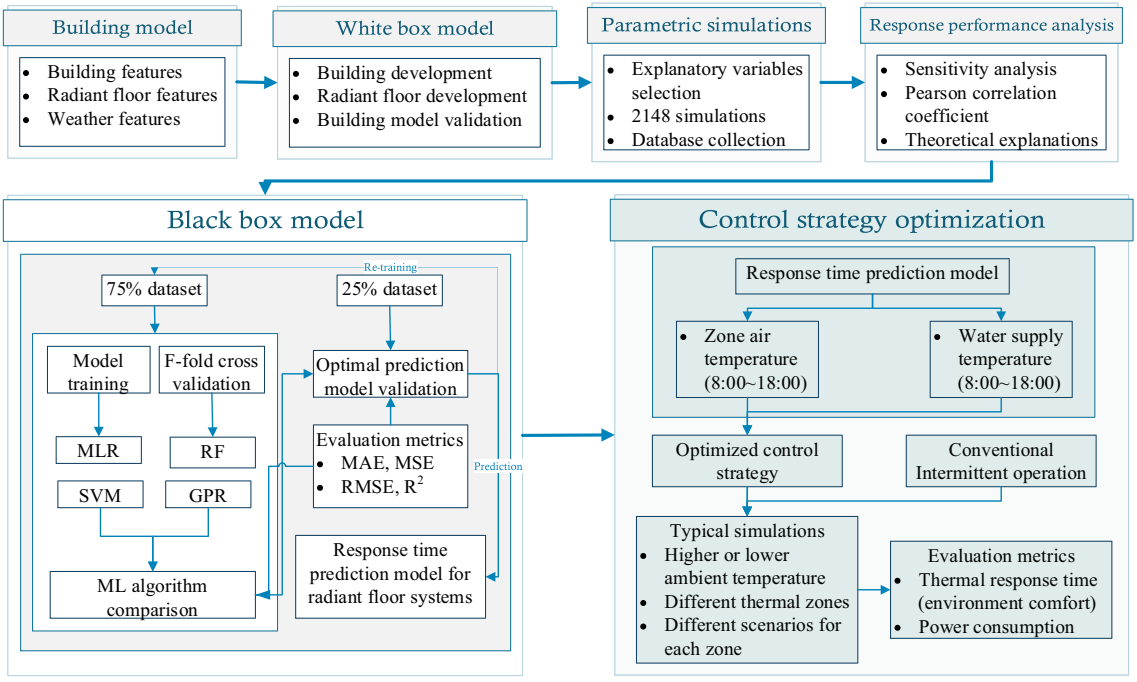

Fig. 1. The flow chart of the research.

which includes three thermal zones of two bedrooms and a living room. The building envelope and configuration design have fulfilled the required energy-saving standard and laws in this area. The total area of the residential building is 50 m^2 and the heating pipes buried area is 40 m^2 which accounts for about 80% of the flooring area. The indoor configurations and the design of the heat radiator are shown in Fig. 11 and Fig. 12 in the control strategy optimization section. Consequently, this information has not to be repeated in this section. The pipe spacing, the pipe diameter, the pipe wall thickness, the thermal property, and the ambient conditions of the building envelopes are shown in Table 1. The building model scheme for simulation in the TRNSYS environment is displayed in Fig. 2. The ambient temperature, relative humidity, and solar radiation recorded by the meteorological stations were used for the simulation boundary. The infiltration loss was assumed as 1 times/h according to the building design description. No occupancy and other equipment heat gain were involved during the experimental period.

The dynamic simulation result can be guaranteed after the reliable base case building calibration. The interior surface tempera-

Table 1
The pipe spacing, the pipe diameter, the pipe wall thickness, the thermal property, and the ambient conditions of the building envelopes information.

Envelopes	Material	Heat transfer coefficient ($W/m^2 \cdot K$)	Thermal resistance($m^2 \cdot K/W$)
Exterior Walls	Cement mortar 20 mm Inorganic insulation mortar 30 mm Sintered shale porous brick masonry 240 mm Cement mortar 20 mm	1.10	0.91
Partition walls	Cement mortar 20 mm Sintered shale porous brick masonry 240 mm Cement mortar 20 mm	1.46	0.69
Floor	Ceramics 10 mm Active layer for heating Concrete backfills 50 mm XPS 20 mm Cement mortar 20 mm Reinforced concrete 120 mm Cement mortar 20 mm	0.99	1.01
Door	Wooden doors	2.47	0.40
Exterior Windows	Plastic window frames (25% of window frame area) 6 + 9A + 6 double glazing	2.50	0.40
Pipe spacing	100 mm	Pipe wall thickness	1.2 mm
Pipe diameter	16 mm		
Average ambient temperature	11.7 °C	Average relative humidity	81%
Maximum solar radiation	610 W/m^2		

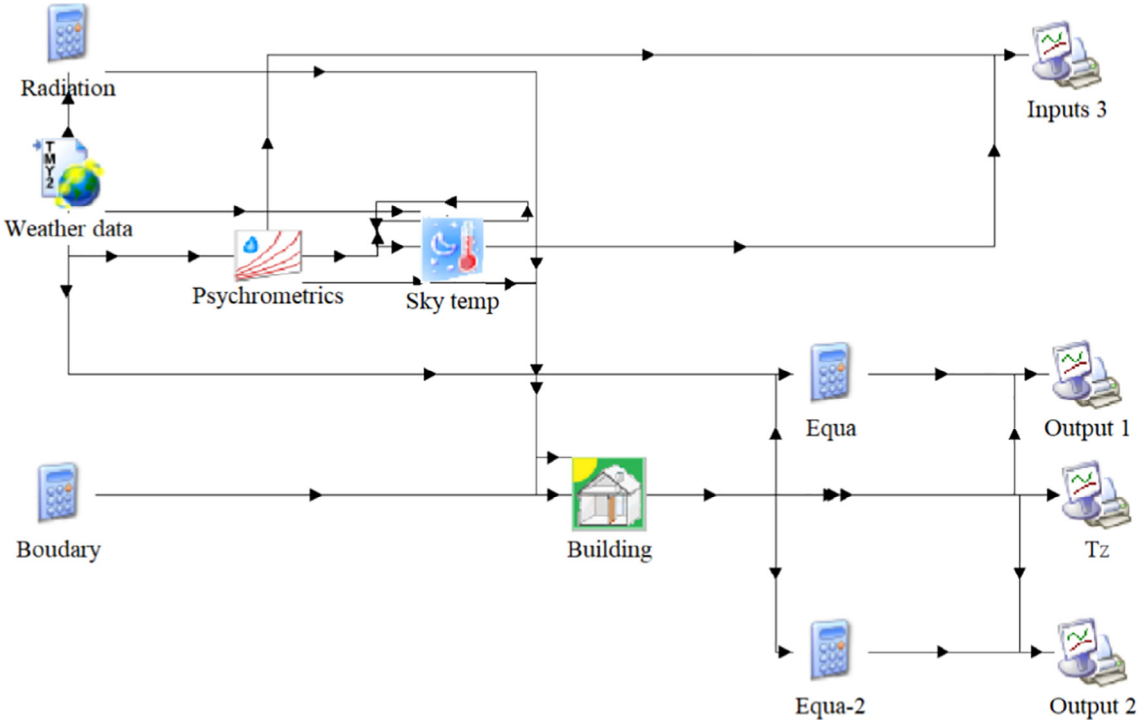

Fig. 2. The building model scheme for simulation in TRNSYS environment.

tures of the building envelop and the vertical zone air temperatures at different heights were monitored with a 5-minute interval and measured by T-Type thermocouples with a relative percentage of less than 5%, which fulfilled the error limitations for effective validation. The T-Type thermocouples measured the height of 1.1 m to the floor and the interior surfaces of thermal zones. The T-Type has been validated by the thermostatic sink for ensuring measurement accuracy. The comparison between the experimental and simulated radiant floor surface temperatures and zone air temperatures is illustrated in Fig. 3 and Fig. 4, respectively. Two error indicators of the mean bias error (MBE) and the coefficient of variation of the root mean square error (CV(RMSE)) are considered and calculated for the base case building validation according to the credible standards and guidelines including the ASHRAE Guideline 14 [42], Measurement and Verification of Federal Energy Projects (FEMP) [43], and International Performance Measurement and Verification Protocol (IPMVP) [44].

The two error indicators of MBE and CV(RMSE) [45,46] were calculated by using the formulae (1) and (2). The calibration criteria of the credible standards and guidelines and two calculated error indicators for the base case calibration are shown in Table 2. MBE and CV(RMSE) of the radiant floor surface temperatures and the zone air temperatures are within the applicable ranges of the credible standards and guidelines mentioned above.

$$\mathrm{MBE} = \frac{\sum_{i=1}^{N}(M_i - S_i)}{\sum_{i=1}^{N} M_i} \tag{1}$$

$$\mathrm{CV(RMSE)} = \frac{\sqrt{\sum_{i=1}^{N}((M_i - S_i)^2/N)}}{\frac{\sum_{i=1}^{N} M_i}{N}} \tag{2}$$

Where M_i and S_i are the measured and simulated data at the instant *i*, respectively. N is the number count of the calibration values.

2.2. Parametric simulation

A reliable database should be obtained for the development of high-fidelity prediction models for thermal response times of radiant floor heating systems. A variety of explanatory variable scenarios are developed for the comparative consideration of the influential factors including boundary conditions such as water supply temperature, ambient temperature, buried pipe specifications. In this research, the main influential factors of the thermal response performance of the radiant floor are considered into concern including the pipe diameter, the pipe spacing, the water supply temperature, the water velocity.

$$T_{resp} = \begin{cases} Q_{heatload} \\ Q_{supply} \end{cases} = \begin{cases} f(T_{amb}, T_{zi}, S/V, Q_{equip}, Q_{infiltration}, Q_{solar}) \\ f(T_{ws}, \vartheta_w, d_o, d_x, d_{filler}) \end{cases} \tag{3}$$

The influential factors contribute to the thermal response time of radiant floors preliminarily estimated as Eq. (3). The response time of radiant floors largely depends on the building energy performance and heat supply capacity of radiant floors. The building energy performance can be correlated with $T_{amb}, T_{zi}, S/V, Q_{equip}, Q_{infiltration}, Q_{solar}$ etc. by using the regression analysis based on reliable database collection in previous research [47]. The heat supply capacity of radiant floors can be estimated as a predictive function of parameters such as $T_{ws}, \vartheta_w, d_o, d_x, d_{filler}$, etc. by applying a variety of intelligent algorithms [48,49] or regression algorithms [18]. The construction methods for radiant floor systems are mainly divided into the floating screed floor radiant heating and pre-grooved insulation board floor radiant heating,

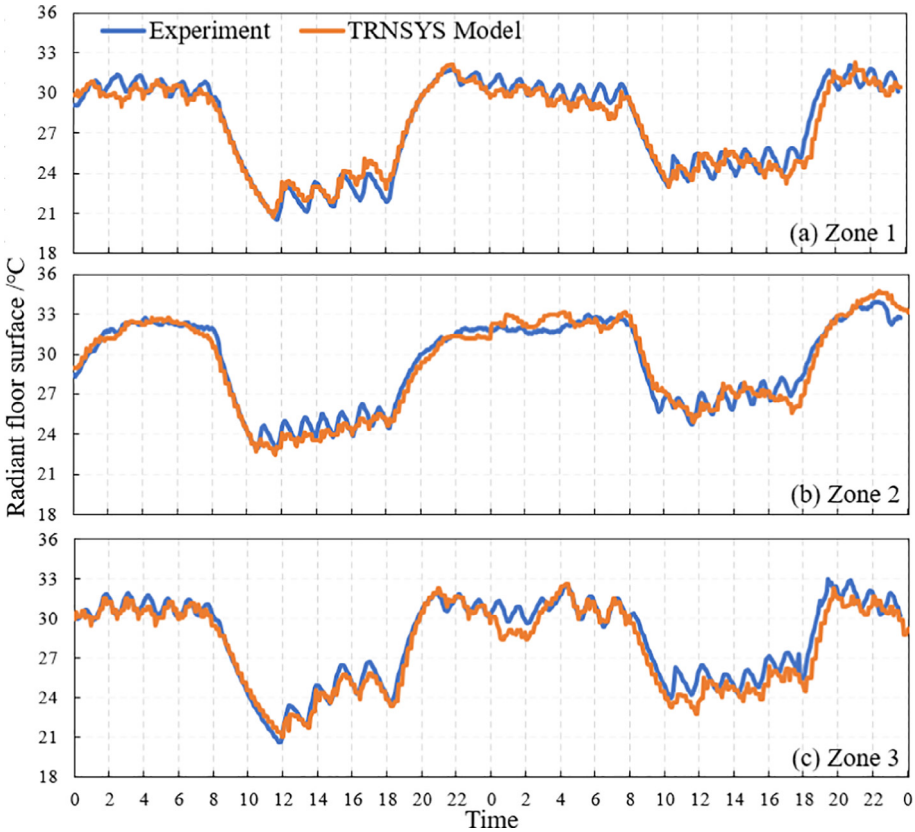

Fig. 3. The comparison between the experimental and simulated radiant floor surface temperatures.

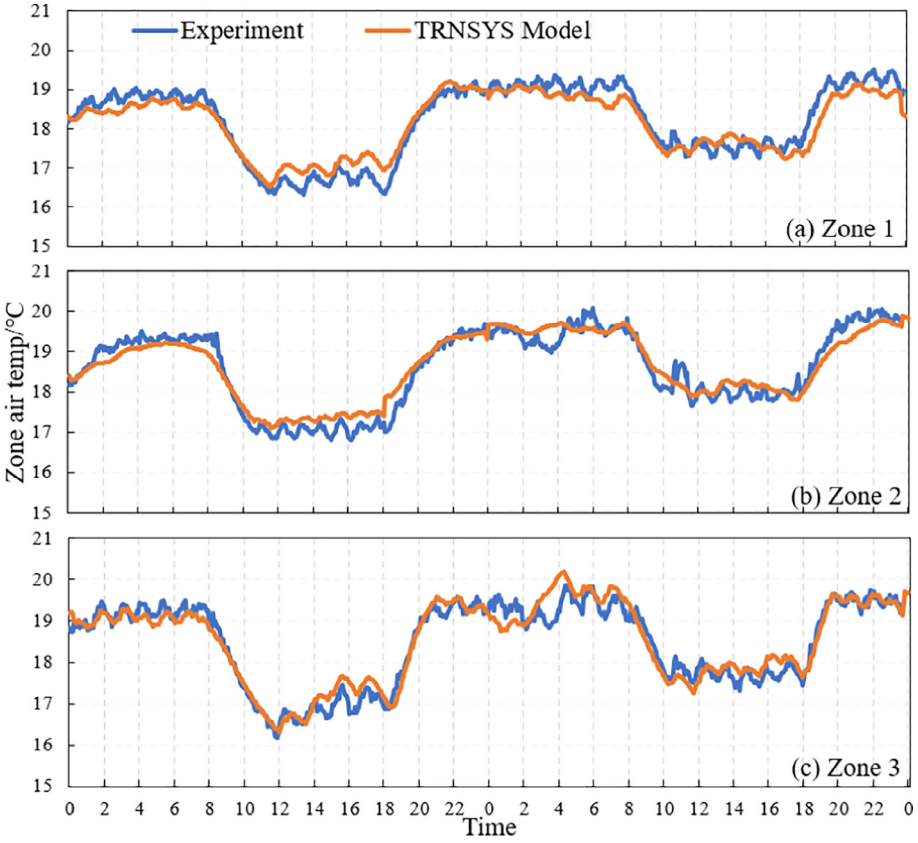

Fig. 4. The comparison between the experimental and simulated zone air temperatures.

Table 2
The calibration criteria of the credible standards and guidelines, and two calculated error indicators for the base case calibration.

Calibration Criteria	Indicator	ASHRAE	FEMP	IPMVP
Criteria (%)	MBE	±10%	±10%	±5%
	CV(RMSE)	30%	30%	20%
Base case	T_{floor}		T_{zone}	
	MBE	CV(RMSE)	MBE	CV(RMSE)
Zone 1	1.67%	2.87%	1.34%	2.65%
Zone 2	1.34%	2.35%	−1.16%	2.50%
Zone 3	1.77%	3.10%	−1.19%	2.46%

and the former is considered as the research objective due to the lower investment, better thermal insulation performance, and advanced construction technology. The filler course for the floating screed floor radiant heating is required to be more than 50 mm according to the standard limitations and it is assumed constant at 50 mm which is made of cement mortar since the larger filler course thickness causes worse heat transfer and thermal response performance.

Besides, the ambient temperature, the initial air temperature, and the shape factor can characterize the heat load of the building envelopes during the response time. In summary, the pipe diameter, the pipe spacing, the water supply temperature, the water velocity, the ambient temperature, the initial zone air temperature, and the shape factor are selected as the main influential and explanatory variables for the parametric simulation scenarios, which is shown in Table 3.

Table 3
The explanatory variables for the parametric simulation.

Explanatory variables	Level 1	Level 2	Level 3
Pipe diameter (mm)	16	20	25
Pipe spacing (mm)	50	100	150
Water velocity (m/s)	0.8	1	1.2
Water supply temperature (°C)	40	45	50
Initial zone air temperature (°C)	15	16	17
Ambient temperature (°C)	5	7	10
Shape factor	0.20	0.26	0.45

The commonly used pipe diameters for radiant pipes are 16 mm, 20 mm, and 25 mm. The three levels of pipe spacing are selected for simulation since the smaller pipe spacing of 20 mm is not suitable for the situation of 25 mm pipe diameter and the larger pipe spacing of more than 150 mm will cause the intense inhomogeneous distribution of radiant floor surface temperatures and insufficient heating capacity. The water velocity is required to be more than 0.25 m/s in the radiant pipe and 0.8 m/s, 1 m/s, 1.2 m/s are typically employed and selected for simulation according to the pre-test results of different water velocity situations. The water supply temperatures of 40 °C, 45 °C, 50 °C are obtained as this research aims at the thermal response performance of radiant floors which undoubtedly requires relatively higher water temperature in this heating phase and lower water temperature such as 35 °C will cause the far lower heat capacity supply and extremely

larger response time. The higher initial zone air temperature means lower peak heat load in the thermal response phase and leads to a smaller response time for the zone air temperature to reach the setpoint. And the lowest initial zone temperature during the intermittent period from 8:00 to 18:00 was around 15 °C in the experiments and pre-simulations. This is the reason why initial zone air temperatures of 15 °C, 16 °C, 17 °C are identified. And the measured ambient temperatures ranged from 5 °C to 10 °C in winter in the experiments and the shape factors of 0.2, 0.26, 0.45 are also considered as the main influential variable since it has a significant impact on building energy performance demonstrated in previous literature which has also presented the negligible influence of other variables such as solar radiation [47]. Therefore, a total of 2148 simulation results covering different explanatory variable combinations is collected for further research on the thermal response performance of radiant floor heating systems.

2.3. Sensitivity analysis

Before the black-box model development of the response time prediction, it is crucial to guarantee the dependence among all the selected explanatory variables. An autocorrelation plot, Pearson and Spearman correlation coefficients, and the clustering methods are the widely used methods for variable dependency recognition. The Pearson correlation coefficients are applied in this research and the correlation matrices among explanatory and response variables are shown in Fig. 5. The Pearson correlation coefficients ranged between −0.002 and 0.047 which explained the entire dependency and their negligible collinearity among selected explanatory variables. Besides, the initial zone air temperature is the most dominating variable for the thermal response time of radiant floor systems demonstrated by the largest Pearson correlation coefficient of −0.604. This is consistent with common sense that higher initial zone air temperature leads to rapid thermal response and shorter response time. Then, the pipe spacing, the water supply temperature, and the shape factor have the following comparative influence on the response time which is also consistent with the intuitive experimental and simulation results. The twice larger pipe spacing of 100 mm is capable of far lower heat supply and the response time is highly longer than that of 50 mm pipe spacing. Therefore, the pipe spacing and the response time are positively correlated. The higher water supply temperature will cause the rapid radiant floor surface temperature and zone air temperature to rise. The larger shape factor of buildings represents the higher heat load compared with that with smaller ones and it takes more response time for the radiant floor heating system to reach the design conditions. Moreover, the pipe diameter and ambient temperature are less related to the response time demonstrated by the relatively smaller Pearson correlation coefficients. And the water velocity has the lowest and negligible impact on the response time indicated by the Pearson correlation coefficient of −0.06 which identifies that increasing the water flow rate is an ineffective approach to improve the radian floor response.

3. Development of response time prediction model

3.1. Gaussian process regression

Gaussian Process Regression (GPR) is a non-parametric model that uses a Gaussian Process (GP) before data regression analysis. The GPR model assumptions include both noise (regression residuals) and Gaussian process prior and its solution is performed by Bayesian inference. GPR is theoretically a universal approximator for any continuous function in the compact space without restricting the kernel function forms. Considering the training set extracted from an unknown distribution, the GPR model solves the problem of predicting the values of the response variables

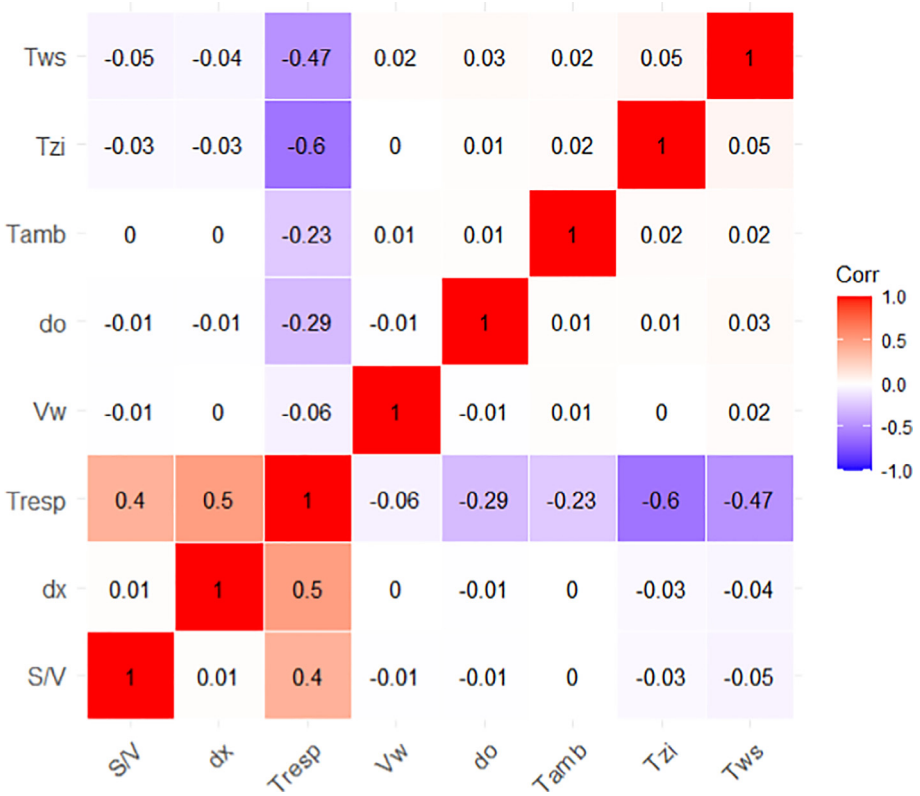

Fig. 5. Correlation matrices among explanatory and response variables.

under the new input vector and training data. A linear regression model takes the following form.

$$y = x^T\beta + \varepsilon \tag{4}$$

where $\varepsilon \in N(0,\sigma^2)$ and the error variance σ^2 and the coefficient β are estimated from the data. The GPR model explains the response $f(x_i), i = 1,2,\cdots,n.$ by introducing a Gaussian process (GP) latent variable and an explicit basis function h. The covariance function of the latent variable captures the smoothing properties of the response, and the basis function projects the input $\times$ into a p-dimensional feature space. GP is a set of random variables such that any finite number of random variables have a joint Gaussian distribution.

If $\{f(x), x \in R^d\}$ is a GP, then n observations $x_1, x_2, \cdots, x_n$ are given, and joint distribution of random variables $f(x_1), f(x_2), \cdots, f(x_n)$ is Gaussian. Now consider the following model.

$$h(x)^T\beta + f(x) \tag{5}$$

where $f(x)$ $GP(0, k(x,x'))$, that is, $f(x)$ comes from a zero-mean GP with a covariance function $k(x,x')$. $h(x)$ is a set of basic functions that transform the original feature vector $\times$ in R^d into a new feature vector h(x) in R^p. This model represents a GPR model. An instance of the response y can be modeled as follows.

$$P(y_i|f(x_i), x_i)\ N(y_i|h(x_i)^T\beta + f(x_i), \sigma^2) \tag{6}$$

Therefore, there is a latent variable $f(x_i)$ introduced for each observation x_i which makes the GPR model nonparametric. In vector form, this model can be transformed into the following.

$$P(y|f,X)\ N(H\beta + f, \sigma^2 I) \tag{7}$$

Where $\mathrm{X} = \begin{pmatrix} \mathrm{x}_1^{\mathrm{T}} \\ \mathrm{x}_2^{\mathrm{T}} \\ \vdots \\ \mathrm{x}_n^{\mathrm{T}} \end{pmatrix}$, $\mathrm{y} = \begin{pmatrix} \mathrm{y}_1 \\ \mathrm{y}_2 \\ \vdots \\ \mathrm{y}_n \end{pmatrix}$, $\mathrm{H} = \begin{pmatrix} \mathrm{h}(\mathrm{x}_1^{\mathrm{T}}) \\ h(\mathrm{x}_2^{\mathrm{T}}) \\ \vdots \\ h(\mathrm{x}_n^{\mathrm{T}}) \end{pmatrix}$, $\mathrm{f} = \begin{pmatrix} \mathrm{f}(\mathrm{x}_1) \\ \mathrm{f}(\mathrm{x}_2) \\ \vdots \\ \mathrm{f}(\mathrm{x}_n) \end{pmatrix}$.

The joint distribution of latent variables $f(x_1), f(x_2), \cdots, f(x_n)$ in the GPR model is described as follows.

$$P(f|X)\ N(f|0, K(X,X)) \tag{8}$$

Where $K(X,X) = \begin{pmatrix} k(x_1,x_1) & \cdots & k(x_1,x_n) \\ \vdots & \ddots & \vdots \\ k(x_n,x_1) & \cdots & k(x_n,x_n) \end{pmatrix}$.

The covariance function $k(x,x')$ is usually parameterized by a set of kernel parameters or hyperparameters, θ. $k(x,x')$ is often written as $k(x,x'|\theta)$ to explicitly indicate the dependence on θ. The basis function coefficients β, the noise variance σ^2, and the hyperparameters θ, of the kernel function from the data can be estimated while training the GPR model. The principal description of the GPR model can trace back to the MATLAB documents [50].

3.2. Performance comparison of ML algorithms

The commonly used ML algorithms for the response time prediction of radiant floor heating systems are developed and evaluated after the parametric simulation collection. There are a variety of alternative ML algorithms that have been successfully employed in the previous research on building energy performance and other aspects except for GPR [51]. There are merits and demerits for these ML algorithms depending on the research objective and application situations. Multiple linear regression (MLR) is applied largely in the field of building energy performance models with simple configuration procedures and no expertise experience based on the extensive data collection which cannot be a solution for explaining and predicting the strongly nonlinear problems. Genetic algorithm (GA) is a powerful optimization method applied in the building energy performance sector and others derived from Darwin's evaluation theory, which can address the complicated problem and give a couple of alternative solutions. However, a single genetic algorithm code does not provide a comprehensive representation of the optimization problem. Genetic algorithms also tend to converge prematurely and are usually less efficient than other traditional optimization methods.

Besides, artificial neural network (ANN) is a popular optimization method in the field of building energy performance. The exhausted database collection and time-consuming pretreatment process required by ANN is indeed crucial for the great reliability and enough accuracy of the developed building energy performance while the reliable and broad enough database is also demanded, although it has been widely employed and excellent with dealing with complicated and non-linear model configuration problem. Moreover, RF which has a wide range of applications is an algorithm that integrates multiple trees through the idea of integration learning. method. It has excellent accuracy and can handle input samples with high-dimensional features without requiring dimensionality reduction. SVM is a class of generalized linear classifiers that performs binary data classification in a supervised learning manner. The optimization problem of SVM considers both empirical and structural risk minimization and is therefore stable.

In this section, the predictive performances of these ML algorithms including MLR, RF, SVM, and GPR are compared and evaluated after the corresponding models are developed. All these algorithms programming has been finished in MATLAB. Then a comparative accuracy is obtained for the response time prediction model for radiant floor heating systems. The dataset obtained from the parametric simulations is divided into two sections while 75% of the dataset is used for model training and 25% of it is applied for model validation. The overfitting problem is a frequent problem during the ML model training, which means that the trained model cannot predict the situation outside the training dataset even though it can match the training data well. Some of the data information known at the time of training will affect the accuracy of the final evaluation results when using test data to tune the model parameters. It is a common practice to subdivide the training data into a portion as validation data, which is used to evaluate the training model performance. In this study, five-fold cross-validation is used for model construction. The principle of five-fold cross-validation is to divide the training dataset into five equal parts and use one of them as the test data and the other four as the training data. The five-fold cross-validation requires five training and validation processes to ensure that all five parts of the data have been involved in the model training. The five models are evaluated separately in the validation set, and the final evaluation errors are summed and averaged to obtain the cross-validation errors.

The comparison results between predicted values and actual values of the thermal response times based on four typical kinds of ML algorithms are shown in Fig. 6. SVM and GPR can achieve better response time prediction performance while MLR and RF are less sensitive and insufficient to demonstrate the response time prediction models. The predicted and actual values can be consistent with each other greatly when the response time is less than 200 min. The predicted value gradually tended to be less than the actual one for MLR and the predicted value deviated from the actual one at a larger scale for RF, while the prediction models based on SVM and GPR can also demonstrate the actual response time trends with few and acceptable discrepancies. Besides, the residual results between predicted values and actual values of the thermal response times based on four typical kinds of ML algorithms are shown in Fig. 7. The discrepancies between actual and

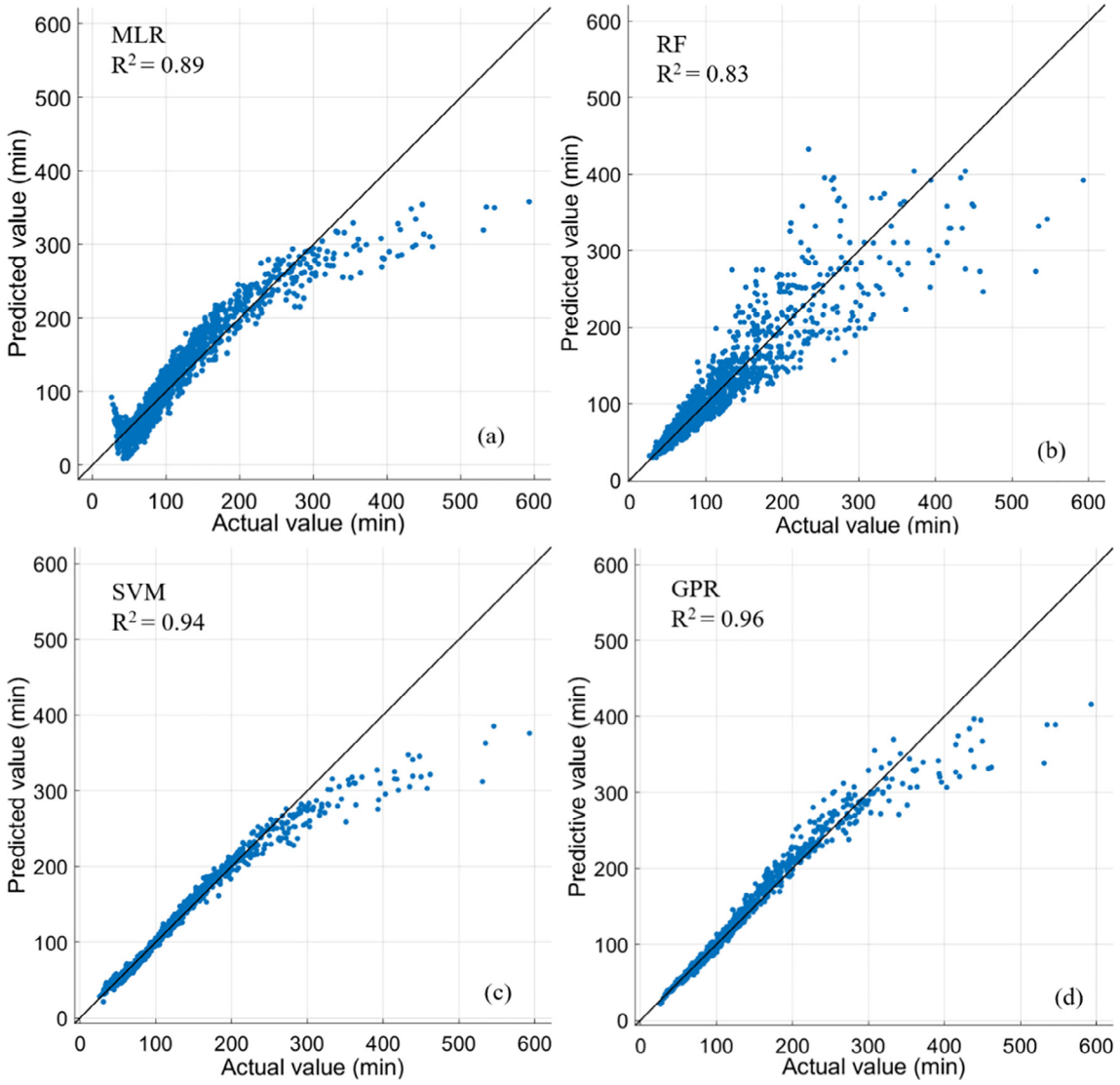

Fig. 6. Comparison results between predicted values and actual values of the thermal response times based on four typical kinds of ML algorithms.

predicted values are illustrated intuitively and clearly. The residual values of MLR and RF were largely higher than that of SVM and GPR during both short-period and long-period response time.

Comprehensive statistical analysis on predictive model accuracy is evaluated by five evaluation criteria displayed as follows, which provide the quantitative support for the alternative high-fidelity black-box model selection.

$$\mathrm{MAE} = \frac{1}{N}\sum_{i=1}^{N}|M_i - S_i| \tag{9}$$

$$\mathrm{MSE} = \frac{1}{N}\sum_{i=1}^{N}(M_i - S_i)^2 \tag{10}$$

$$\mathrm{RMSE} = \sqrt{\frac{1}{N}\sum_{i=1}^{N}(M_i - S_i)^2} \tag{11}$$

$$R^2 = 1 - \frac{\sum_{i=1}^{N}(M_i - S_i)^2}{\sum_{i=1}^{N}\left(M_i - \bar{M}_i\right)^2} \tag{12}$$

Evaluation results of four ML models based on metrics of MAE, MSE, RMSE, and R^2 are shown in Fig. 8. The GPR algorithm achieved the best predictive performance among all the analyzed ML algorithms with the lowest MAE, MSE, RMSE (5.89, 215.88, 14.69), and highest R^2 (0.96). The SVM algorithm had the slightly comparative performance of the response time predictive model with higher MAE, MSE, RMSE (6.92, 308.25, 17.56), and lower R^2 (0.94). The MLR algorithm had the satisfactory performance of the response time predictive model with MAE, MSE, RMSE (16.27, 619.61, 24.89), and R^2 (0.89). The RF algorithm failed to characterize the response time performance of radiant floor heating systems with the highest MAE, MSE, RMSE (17.42, 926.11, 30.43), and lowest R^2 (0.83). Therefore, the GPR model is selected for the response time prediction of radiant floor heating systems due to the optimal regression performance.

3.3. GPR model validation

As mentioned before, 25% of the dataset was retained for the model validation while 75% of that was used for model training and cross-validation. The prediction accuracy can be evaluated through the retained dataset without involving the model develop-

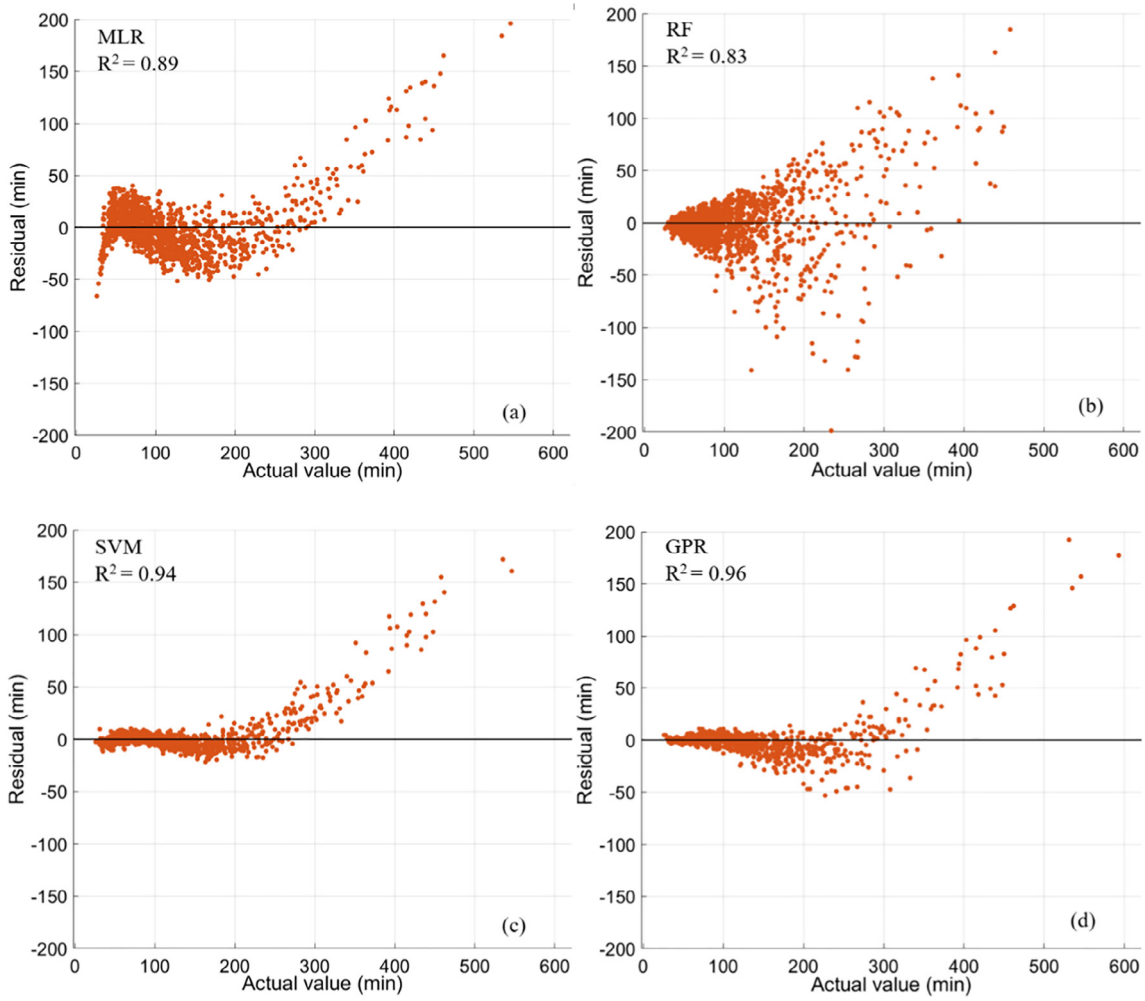

Fig. 7. Residual results between predicted values and actual values of the thermal response times based on four typical kinds of ML algorithms.

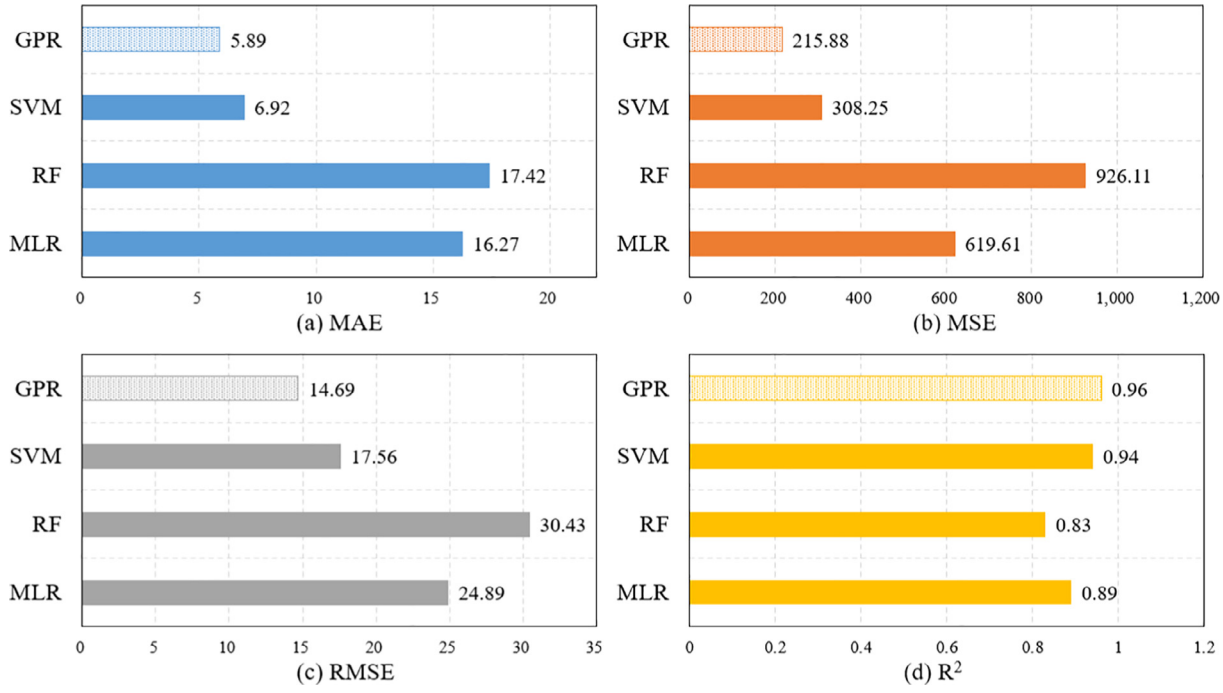

Fig. 8. Evaluation results of four ML models based on metrics of MAE, MSE, RMSE, and R^2.

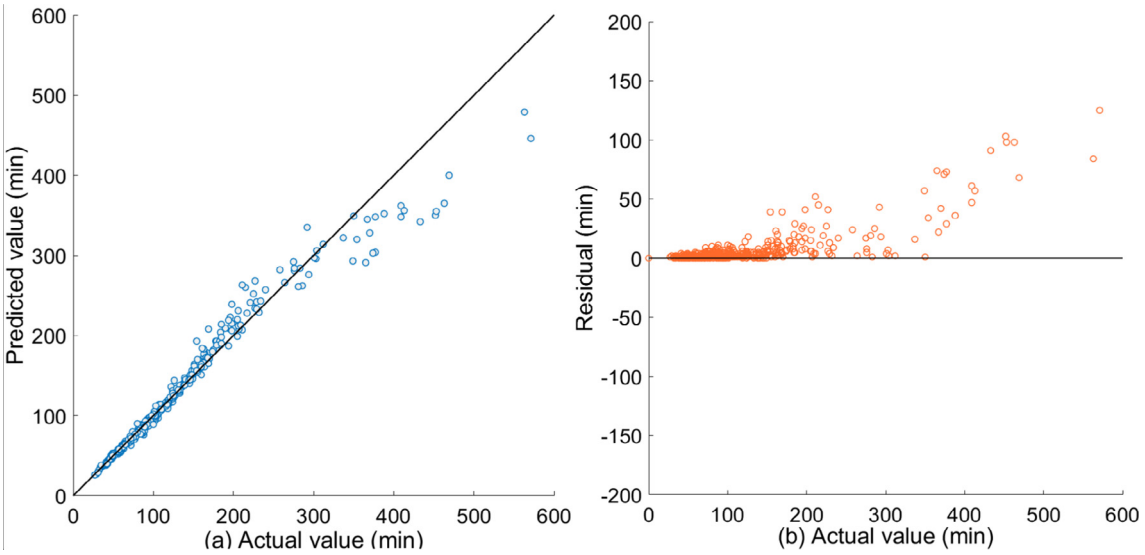

Fig. 9. The prediction and residual results of the validation dataset.

ment which is judged by those metrics indicated before. The prediction and residual results of the validation dataset are shown in Fig. 9. The excellent consistency between predicted and actual values and almost few residuals confirmed the great accuracy and applicability of the GPR model for the response time prediction. Furthermore, the quantitative evaluation metrics of MAE, MSE, RMSE (6.10, 241.38, 15.54), and R^2 (0.96) highly close to the training model evaluation results also contributed to the high-fidelity model validation.

4. Control strategy optimization

Heat capacity and time-lag effects are important indicators to be considered in the performance analysis of radiant heating systems during the design and operation phases [3]. To improve the heating capacity of radiant heating systems, researchers have proposed various approaches such as adding coatings to the surface [52], changing the internal structure of radiant heating panels [3,53], and increasing convective heat transfer on the surface of radiant floors [54,55]. In addition, the thermal inertia of radiant flooring is also an important factor affecting the performance of the control system, and new radiant flooring is also trying to reduce its thermal inertia by simplifying the structure of the floor, to improve the thermal response speed of the radiant flooring system [56]. The long thermal response time of the radiant floor heating system under intermittent operation due to the high thermal inertia means that the indoor thermal comfort is far below the demand level of indoor occupants during the thermal response period. The long thermal response time of the radiant floor heating system caused the serious overshoot and delay of the zone air temperature regulation and control. To address this issue, the optimized thermal repose time prediction-based control strategy for radiant floor heating systems by applying GPR is proposed as illustrated in Fig. 10, which can predict the water supply temperature and initial zone air temperature in advance that can afford to the peak heat load supply at 18:00 (system starts running) and guarantee the acceptable thermal response time according to the response time prediction model.

Firstly, a reliable GPR black-box model based on the explanatory variables mentioned above was developed to predict thermal response times for different ambient environments, radiant floor configurations, and building envelope characteristics in the above

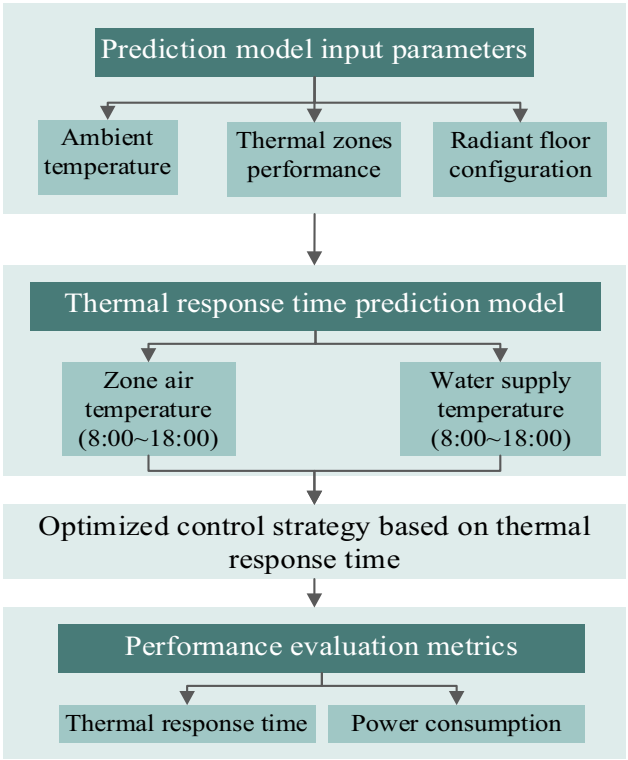

Fig. 10. The optimized thermal repose time prediction-based control strategy for radiant floor heating systems by applying the Gaussian process algorithm.

sections. After that, the forecast weather information, the specific building envelope, and radiant floor configurations are identified and used to predict the demand zone air temperature setpoint (8:00 ~ 18:00) and water supply temperature of the response time to keep the thermal response time within acceptable ranges. Therefore, this proposed optimal control strategy based on the thermal response time prediction model can effectively improve the indoor thermal comfort performance of the radiant floor heating system while reducing the peak load and energy consumption of the system.

The proposed optimized control strategy is evaluated by simulation of the radiant floor heating systems for the thermal response time reduction, environment comfort improvement, and energy efficiency performance. The schematical three-dimensional sketch diagram of the three-zone building with radiant floor heating systems is shown in Fig. 11. The apartment is on the second floor and between two neighboring units. The dimensional geometry, the specific building envelope configuration, and component material have been demonstrated above in the base case calibration. Among all the alternative radiant floor configurations, the pipe diameter and pipe spacing are 0.016 mm and 0.1 mm, respectively. The water flow rates of the three thermal zones are 400 m^3/h, 490 m^3/h, and 350 m^3/h, respectively. The schematic drawing for the radiant floor heating system is shown in Fig. 12. The radiant floor heating system was supplied by the air-source heat pump or the gas-fired furnace. The water tank serves as the heat change media with the water splitter and water mixer which is connected with the terminal radiant floors.

Simulations under different operating conditions were developed to explore the potential of the optimal control strategy based on response time prediction proposed in this study for fast thermal response and energy efficiency in radiant floor heating systems compared to the commonly used intermittent operation. The zone air temperature and water temperature settings of optimized control strategy and intermittent operation under different case studies are shown in Table 4. T_{zi} (The zone air temperature setpoint of the intermittent period 8:00 ~ 18:00) of three zones were the same with each other for case studies one and two where the average ambient temperatures were at the typically higher level of 10.1 °C and relatively lower level of 5.7 °C, respectively. For case study three, T_{zi} of three zones were different from each other which were obtained following their different heat loads. Besides, the energy consumption of the system mainly comes from the air-source heat pump usually integrated into radiant floor heating systems. The power consumption of the air-source heat pump depends on the COP (coefficient of performance), which is related

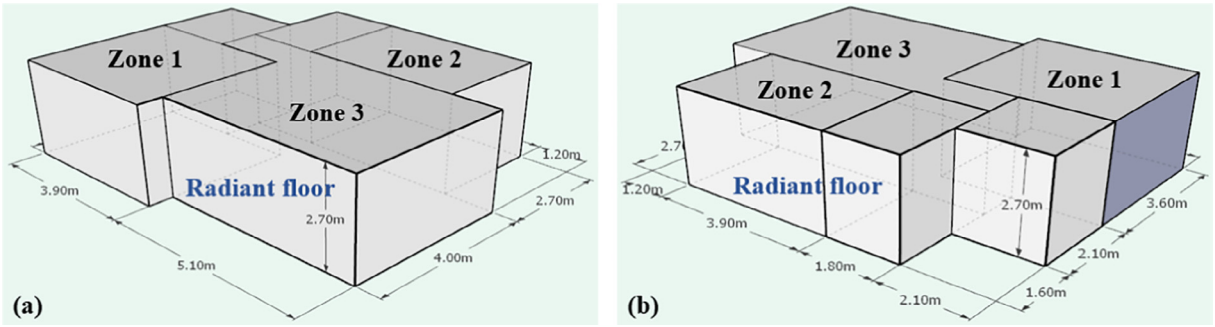

Fig. 11. Schematical three-dimensional sketch diagram of the three-zone building with radiant floor heating systems.

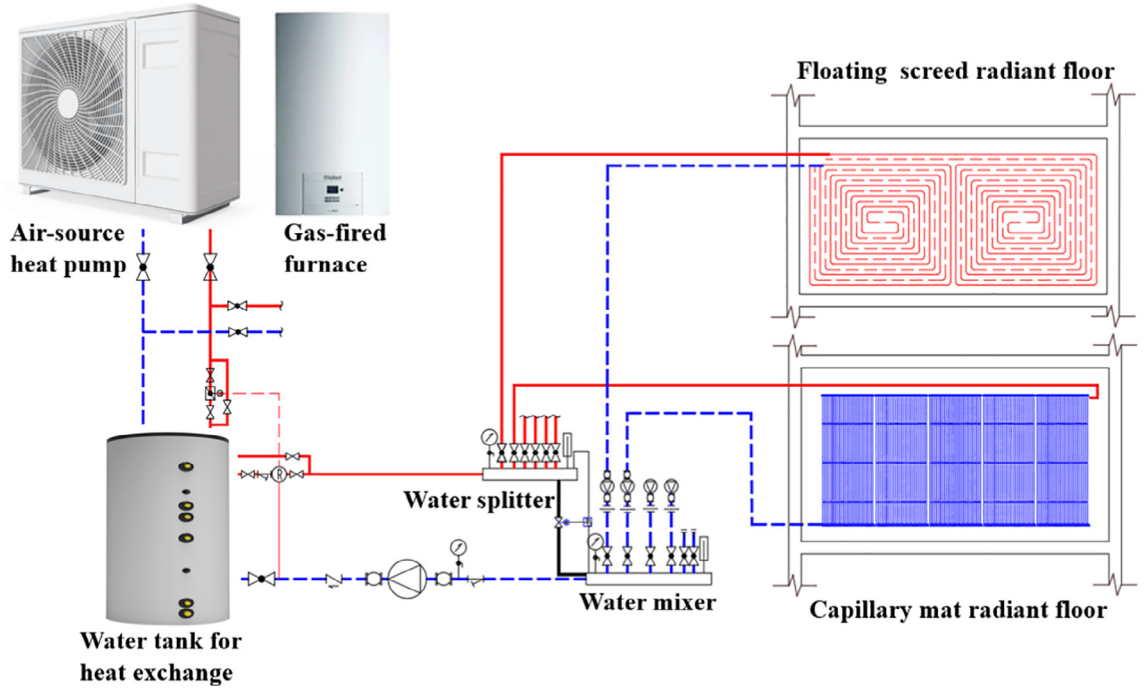

Fig. 12. Schematic drawing for the radiant floor heating system.

Table 4
The zone air temperature and water temperature settings of optimized control strategy and intermittent operation under different case studies.

Case	Control strategy	Items	Intermittent period			Response period	Other periods
Case 1	Optimized control	T_z(°C)	17			18	18
		T_{ws}(°C)	30			45	40
	Intermittent control	T_z(°C)	18				
		T_{ws}(°C)	40				
Case 2	Optimized control	T_z(°C)	17			18	18
		T_{ws}(°C)	30			50	45
	Intermittent control	T_z(°C)	18				
		T_{ws}(°C)	45				
Case 3	Optimized control	T_z(°C)	Zone 1	Zone 2	Zone 3	18	18
			16.5	17	16		
		T_z(°C)	30			50	45
	Intermittent operation	T_z(°C)	18				
		T_{ws}(°C)	45				

to parameters such as water supply temperature and ambient temperature. The fitting results of COP of the air-source heat pump are demonstrated in the following equations.

$$Q_p = Q_h / COP \tag{13}$$

$$\begin{aligned} \mathrm{COP} = {} & 7.691 + 0.4559 * T_a - 0.165 * T_{ws} + 0.001027 * {T_a}^2 \\ & - 0.01567 * T_a * T_{ws} + 0.001192 * {T_{ws}}^2 + 0.0001733 \\ & * {T_a}^3 - 9e - 05 * {T_a}^2 * T_{ws} + 0.000164 * T_a * {T_{ws}}^2 \end{aligned} \tag{14}$$

5. Results and discussion

The simulation results of radian floor heating systems are comprehensively evaluated under the proposed optimized control strategy and compared to that of the intermittent operation in terms of thermal response time and power consumption in this section.

5.1. Lower heat load

In this case, the heat loads for the three thermal zones were relatively lower due to the higher average ambient temperature. To ensure that the thermal response times for the three zones are about one hour, it can be determined that T_{zi} of three zones during the intermittent period (8:00 ~ 18:00) was set at 17 °C. T_{ws} was set at the lower water temperature of 30 °C due to the decreased heat load which is caused by the lower zone air temperature and the higher ambient temperature during the daytime. T_{ws} of the thermal response period (the period from 18:00 to the time when the zone air temperature reached 18 °C) was adjusted upward to 45 °C based on the thermal response prediction model and known information such as the specifications of the radiant floor and the zones configurations. On the other hand, T_z and T_{ws} were set at 18 °C and 40 °C all the time except for the period of the thermal response period and 8:00 ~ 18:00 for the optimized control strategy. T_z and T_{ws} were set at 18 °C and 40 °C all the time except for the period of 8:00 ~ 18:00 under the intermittent operation when the heating system was turned off. The

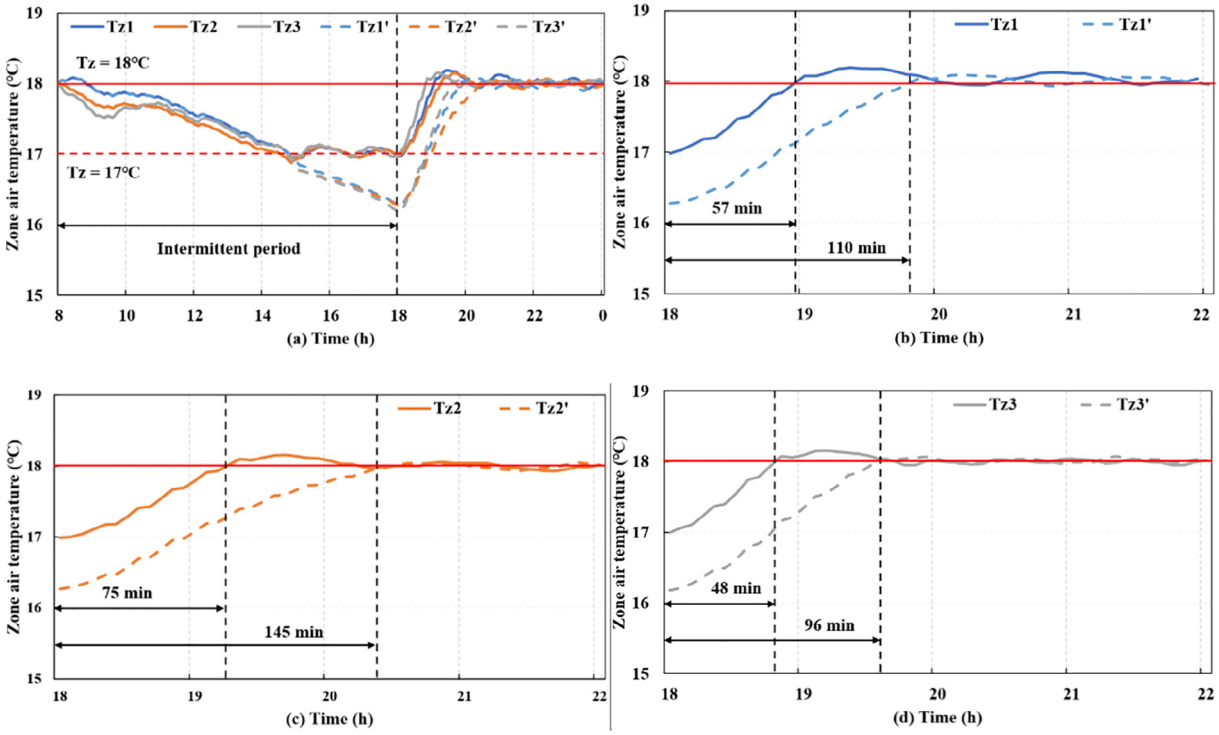

Fig. 13. The zone air temperature trends of the optimized control strategy and the intermittent operation under case study one.

Table 5
The thermal response time of the optimized control strategy and the intermittent operation under different case studies.

Case	Optimized control (min)				Intermittent control	△Tresp2 (min)	△Tresp2 (%)
	Zone	Predicted value	Simulation	ΔT_{resp1}			
Case 1	Zone 1	59	57	−2	110	−53	−48%
	Zone 2	68	75	7	145	−70	−48%
	Zone 3	50	48	−2	96	−48	−50%
Case 2	Zone 1	43	49	6	135	−86	−64%
	Zone 2	70	67	−3	188	−121	−64%
	Zone 3	48	44	−4	120	−76	−64%
Case 3	Zone 1	63	65	2	130	−65	−50%
	Zone 2	65	61	−4	167	−106	−63%
	Zone 3	67	65	−2	110	−45	−41%

Note:$\Delta T_{resp1} = T_{resp}(\text{simulation}) - T_{resp}(\text{prediction})$,
$\Delta T_{resp2} = T_{resp}(\text{simulation}) - T_{resp}(\text{Intermittent})$,
$\Delta T_{resp2}(\%) = (T_{resp}(\text{simulation}) - T_{resp}(\text{Intermittent}))/T_{resp}(\text{Intermittent})$.

zone air temperature trends of the optimized control strategy and the intermittent operation under case study one are shown in Fig. 13 and the thermal response times of the optimized control strategy and the intermittent operation under different case studies are demonstrated in Table 5. The initial air temperatures were significantly higher for the optimized control strategy than that for the intermittent operation, which was the main reason why the thermal response time was remarkably lower in all three thermal zones of the former than of the latter. The thermal response times for the three thermal zones were reduced from 96 ∼ 145 mins to 48 ∼ 75 mins, a reduction of about 48 ∼ 70 mins, or roughly 48% ∼ 50%.

The power consumption of the air-source heat pump of the optimized control strategy and the intermittent operation of case one was illustrated in Fig. 14(a). Overall, the total power consumptions for the three thermal zones under the two control strategies were not significantly different throughout the day. Although there was a small increase in power consumption under the optimized control strategy during the intermittent period compared with the intermittent operation, the optimized control strategy also reduced the peak heat load during the thermal response phase after the 18:00 h. However, the heat load under intermittent operation after the 18:00 h was significantly larger, and the long-time operation under the decreased COP due to the relatively lower ambient temperature led to higher energy consumption under the intermittent operation than that of the optimized control strategy during the thermal response period. The total power consumptions of all the three thermal zones of the optimized control strategy were 1.0% higher than that of the intermittent operation on average.

5.2. Higher heat load

In this case, the heat loads for the three thermal zones were relatively higher owing to the lower average ambient temperature. According to the response time prediction model, it can be determined that T_{zi} of three zones was set at 17 °C and T_{ws} was set at the lower water temperature of 30 °C during the intermittent period (8:00 ∼ 18:00). T_{ws} of the thermal response period was increased upward to 50 °C since the lower ambient temperature contributed to the higher heat load for case two. In addition, T_z and T_{ws} were set at 18 °C and 45 °C all the time except for the period of the thermal response period and 8:00 ∼ 18:00 for the optimized control strategy. T_z and T_{ws} were set at 18 °C and 45 °C all the time except for the period of 8:00 ∼ 18:00 under the intermittent operation when the heating system was turned off. The zone air temperature trends of the optimized control strategy and the intermittent operation under case study two are shown in Fig. 15

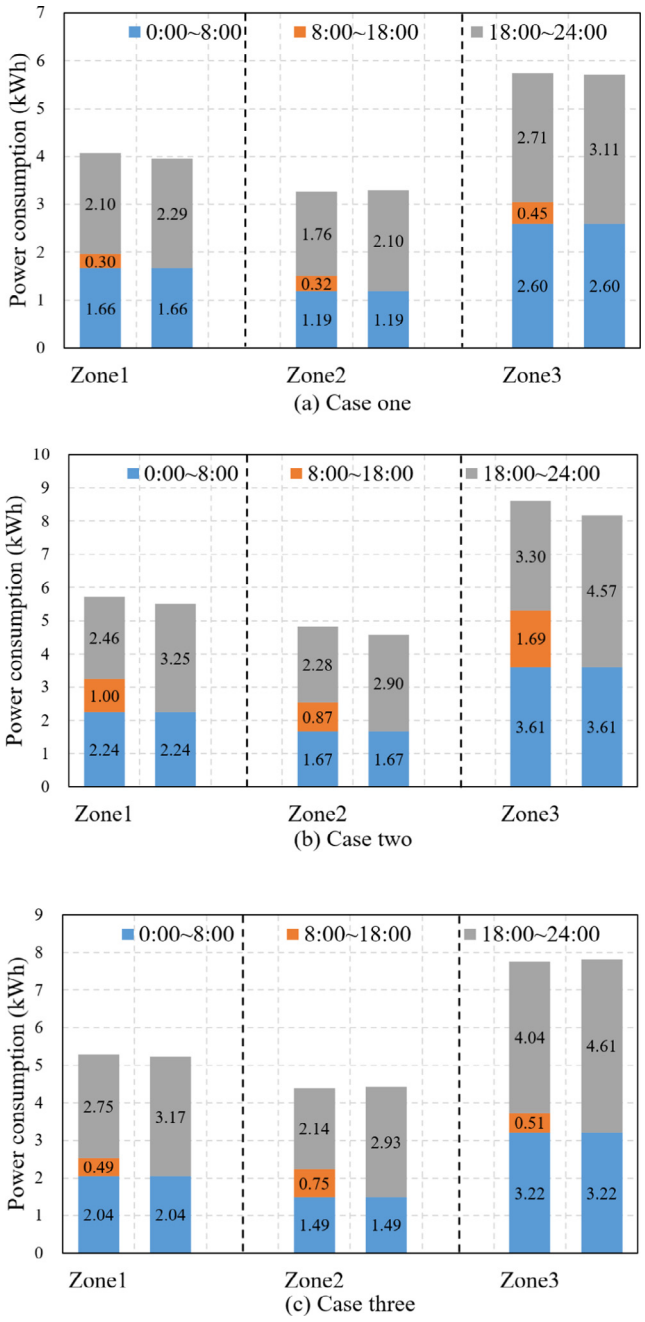

Fig. 14. The power consumption of the air-source heat pump of the optimized control strategy and the intermittent operation under three cases.

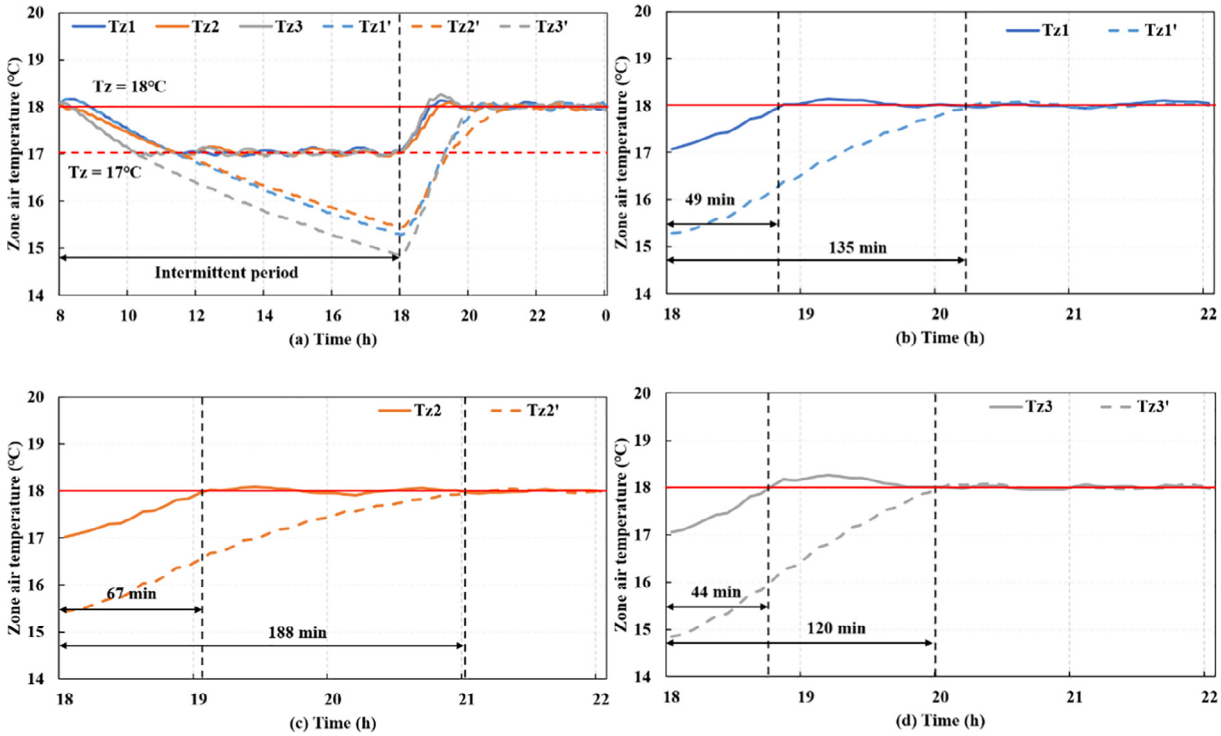

Fig. 15. The zone air temperature trends of the optimized control strategy and the intermittent operation under case study two.

and the thermal response times of the optimized control strategy and the intermittent operation under different case studies are demonstrated in Table 5.

As can be seen, the zone air temperatures quickly decreased to 17 °C and the radiant floor heating system runs continuously from 11:00 to 18:00 due to the lower ambient temperature during the daytime relative to case one. Then the initial air temperatures were 1.5 ∼ 2 °C higher for the optimized control strategy than that for the intermittent operation. And this was also responsible for the significantly increased thermal response time for the intermittent operation. Therefore, the thermal response times for the three thermal zones were reduced from 120 ∼ 188 mins to 44 ∼ 67 mins, a reduction of about 76 ∼ 121 mins, or nearly 64%.

The power consumptions of the air-source heat pump of the optimized control strategy and the intermittent operation of case two were illustrated in Fig. 14(b). Overall, the total power consumptions for the three thermal zones under the two control strategies were almost as large as each other throughout the day. Similar to case one, the total power consumptions of the optimal control strategy were still competitive compared to the intermittent operation due to the large peak load reduction of the former during the thermal response phase although the optimal control strategy undertook on additional power consumption during the intermittent period of 8:00 ∼ 18:00. The total power consumptions of all the three thermal zones of the optimized control strategy were 4.9% higher than that of the intermittent operation on average.

5.3. Case study three

From case one and case two, it can be seen that the thermal response time of the thermal zone two with greater heat load in the same supply temperature was about 35% larger compared to the thermal zone one and thermal zone three, and this problem cannot be better solved by water flow distribution. In case three, T_{zi} of the three thermal zones were set differently according to their heat load to address the problem of the uneven thermal response times of the three thermal zones. According to the response time prediction model, it can be determined that T_{zi} of three zones during the intermittent period (8:00 ∼ 18:00) was set at 16.5 °C, 17 °C, and 16 °C, respectively. T_{ws} was set at 30 °C during the daytime of 8:00 ∼ 18:00. T_{ws} was increased upward to 50 °C during the thermal response period. Besides, T_z and T_{ws} were set at 18 °C and 45 °C all the time except for the period of the thermal response period and 8:00 ∼ 18:00 for the optimized control strategy. T_z and T_{ws} were set at 18 °C and 45 °C all the time except for the period of 8:00 ∼ 18:00 under the intermittent operation when the heating system was turned off.

The zone air temperature trends of the optimized control strategy and the intermittent operation under case study three are shown in Fig. 16 and the thermal response times of the optimized control strategy and the intermittent operation under different case studies are demonstrated in Table 5. The three thermal zones were heated at zone air temperatures of 16.5 °C, 17 °C, and 16 °C for 5 h, 6 h, and 4 h, respectively during 8:00 ∼ 18:00. The thermal response times for the three thermal zones were reduced from 110 ∼ 167 mins to 61 ∼ 65 mins, a reduction of about 45 ∼ 106 mins, or roughly 41% ∼ 63%. Furthermore, the thermal response times difference among the three zones was only 4 min or about 6%.

The power consumptions of the air-source heat pump of the optimized control strategy and the intermittent operation of case three are illustrated in Fig. 14(c). Overall, the total power consumptions for the three thermal zones under the two control strategies were almost as same as each other throughout the day. The zone air temperatures were differently set for the three zones which have further reduced the total power consumptions of the radiant floor heating systems. And the total power consumptions of the optimized control strategy were 0.1% lower than that of the intermittent operation. Consequently, the more rapid ther-

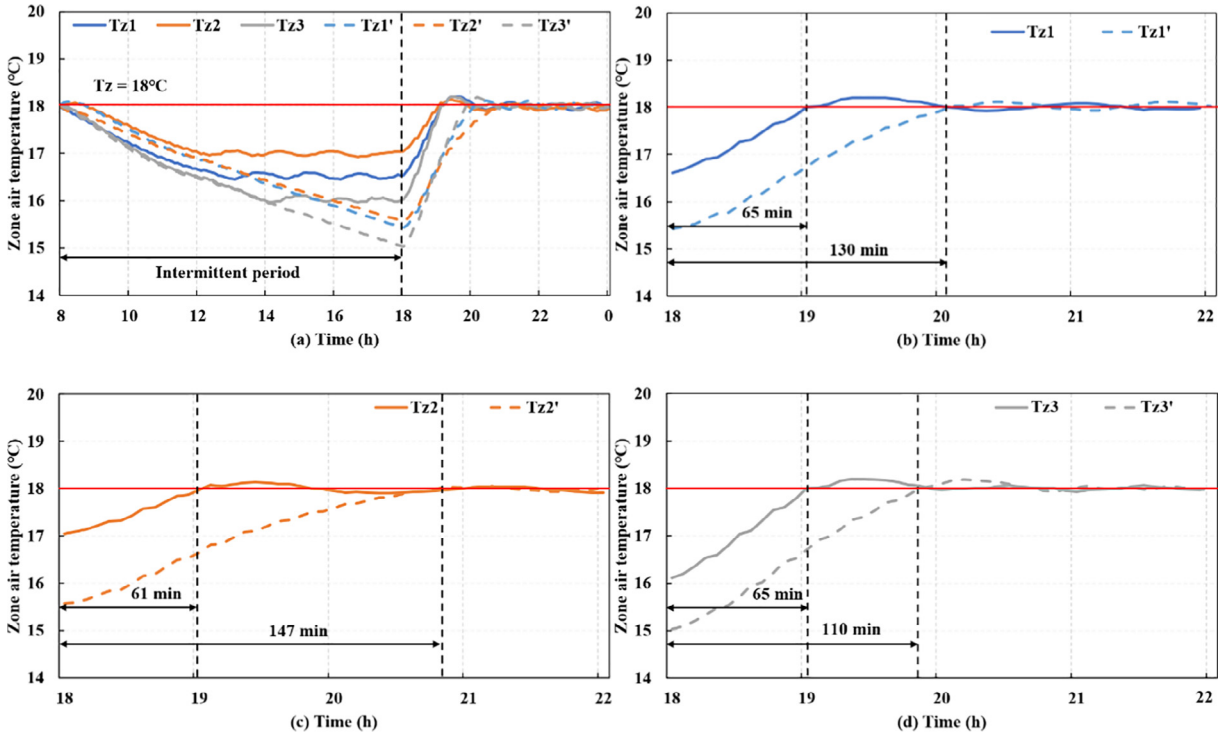

Fig. 16. The zone air temperature trends of the optimized control strategy and the intermittent operation under case study three.

mal response and comparatively power consumption have ensured the great potential of the proposed optimized control strategy based on the thermal response time prediction model in terms of better environment comfort and energy efficiency.

6. Conclusion

In this study, an optimal control strategy based on a thermal response time prediction model for radiant floor heating systems was proposed by applying the GPR algorithm and evaluated by comparison with conventional intermittent operation strategy in terms of rapid response performance and energy efficiency. First, a base case building model was developed by TNRSYS and validated by experimental results. Then, a comprehensive database of thermal response times for a variety of scenarios based on various building characteristics, radiant floor features, and weather information was obtained by parametric simulations. Besides, a sensitivity analysis of the thermal response performance to seven kinds of explanatory variables was performed by introducing Pearson correlation coefficients, and a comprehensive theoretical explanation of the sensitivity analysis results was demonstrated which indicated that the initial zone air temperature, the pipe spacing, the water supply temperature, and the shape factor contributed to thermal response time in descending order while the pipe diameter and the ambient temperature had smaller influence and the water velocity in the buried pipe had few impacts on the thermal response performance of radiant floors. The significance analysis of the characteristic parameters of the radiant floor was obtained to rank the influencing factors affecting the thermal response time of radiant floor which can provide guiding suggestions for the radiant floor heating system design. Moreover, the response time prediction model of radiant floor heating systems based on the GPR algorithm with a larger R^2 of around 0.96 was obtained by an in-depth comparison of commonly used ML algorithms such as MLR, RF, and SVM. And its accuracy was verified by cross-validation and 25% of database collection. Finally, an optimal control strategy based on the response time prediction model was proposed and compared with the conventional intermittent operation strategy in terms of thermal response performance and energy efficiency. The optimized control strategy can reduce the response time from the original 96 $\sim$ 188 mins to about 44 $\sim$ 75 mins, achieving a reduction in thermal response time of 45 $\sim$ 121 mins, a reduction of about 41% $\sim$ 64% while keeping the comparative power consumption. Integrating the thermal response time prediction model into the radiant floor heating control system can effectively preheat the building's indoor environment during the lower electricity consumption periods. The peak load of the radiant floor heating system was reduced while relieving the pressure on the power grid during peak electricity consumption. Therefore, the proposed optimal control of thermal response prediction based on the GPR algorithm can effectively and largely reduce the thermal response time of the radiant floor heating system and improve the indoor thermal comfort during the thermal response phase without sacrificing the power consumption.

Declaration of Competing Interest

The authors declare that they have no known competing financial interests or personal relationships that could have appeared to influence the work reported in this paper.

References

[1] China Urban-Rural Construction Statistical Yearbook 2019.
[2] A. Afram, F. Janabi-Sharifi, Theory and applications of HVAC control systems – A review of model predictive control (MPC), Build. Environ. 72 (2014) 343–355.
[3] K.-N. Rhee, K.W. Kim, A 50 year review of basic and applied research in radiant heating and cooling systems for the built environment, Build. Environ. 91 (2015) 166–190.

[4] J.(. Feng, F. Chuang, F. Borrelli, F. Bauman, Model predictive control of radiant slab systems with evaporative cooling sources, Energy Build. 87 (2015) 199–210.
[5] S. Li, J. Joe, J. Hu, P. Karava, System identification and model-predictive control of office buildings with integrated photovoltaic-thermal collectors, radiant floor heating and active thermal storage, Sol. Energy 113 (2015) 139–157.
[6] J.-H. Lim, J.-H. Jo, Y.-Y. Kim, M.-S. Yeo, K.-W. Kim, Application of the control methods for radiant floor cooling system in residential buildings, Build. Environ. 41 (1) (2006) 60–73.
[7] M.-S. Shin, K.-N. Rhee, G.-J. Jung, Optimal heating start and stop control based on the inferred occupancy schedule in a household with radiant floor heating system, Energy Build. 209 (2020) 109737.
[8] H. Tang, T. Zhang, X. Liu, Y. Jiang, Study on the pulsed flow control on radiant cooling and heating systems in part load, Procedia Eng. 205 (2017) 11–18.
[9] J. Romaní, A. de Gracia, L.F. Cabeza, Simulation and control of thermally activated building systems (TABS), Energy Build. 127 (2016) 22–42.
[10] Y.Q. Xu, Y.T. Peet, Effect of an on/off HVAC control on indoor temperature distribution and cycle variability in a single-floor residential building, Energy Build. 251 (2021) 111289.
[11] Z. Wang, Y. Hang, M. Luo, et al., Predicting older people's thermal sensation in building environment through a machine learning approach: Modelling, interpretation, and application, Build. Environ. 161 (2019) 106231.
[12] K.S. Cetin, M.H. Fathollahzadeh, N. Kunwar, H. Do, P.C. Tabares-Velasco, Development and validation of an HVAC on/off controller in EnergyPlus for energy simulation of residential and small commercial buildings, Energy Build. 183 (2019) 467–483.
[13] G. Ulpiani, M. Borgognoni, A. Romagnoli, C. Di Perna, Comparing the performance of on/off, PID and fuzzy controllers applied to the heating system of an energy-efficient building, Energy Build. 116 (2016) 1–17.
[14] E. Bourdakis, O.B. Kazanci, B.W. Olesen, Load calculations of radiant cooling systems for sizing the plant, Energy Procedia 78 (2015) 2639–2644.
[15] S. Brandi, M.S. Piscitelli, M. Martellacci, et al., Deep reinforcement learning to optimise indoor temperature control and heating energy consumption in buildings, Energy Build. 224 (2020) 110225.
[16] L. Jia, S. Wei, J. Liu, A review of optimization approaches for controlling water-cooled central cooling systems, Build. Environ. 203 (2021) 108100.
[17] Y. Li, Z. Zhuang, Q. Zhu, J. song, H. An, Research on control methods of roof radiant cooling system, Procedia Eng. 205 (2017) 2149–2155.
[18] M. Schmelas, T. Feldmann, E. Bollin, Adaptive predictive control of thermo-active building systems (TABS) based on a multiple regression algorithm, Energy Build. 103 (2015) 14–28.
[19] M. Schmelas, T. Feldmann, E. Bollin, Savings through the use of adaptive predictive control of thermo-active building systems (TABS): a case study, Appl. Energy 199 (2017) 294–309.
[20] M. Gwerder, J. Tödtli, B. Lehmann, V. Dorer, W. Güntensperger, F. Renggli, Control of thermally activated building systems (TABS) in intermittent operation with pulse width modulation, Appl. Energy 86 (9) (2009) 1606–1616.
[21] D. Lee, C.-J. Lin, C.-W. Lai, et al., Smart-valve-assisted model-free predictive control system for chiller plants, Energy Build. 234 (2021) 110708.
[22] K. Ma, M. Liu, J. Zhang, An improved particle swarm optimization algorithm for the optimization and group control of water-side free cooling using cooling towers, Build. Environ. 182 (2020) 107167.
[23] J. Romaní, L.F. Cabeza, A. de Gracia, Development and experimental validation of a transient 2D numeric model for radiant walls, Renewable Energy 115 (2018) 859–870.
[24] W. Song, J. Yang, Y. Ji, et al., Experimental study on characteristics of a dual temperature control valve in the chilled water system of an air-conditioning unit, Energy Build. 202 (2019) 109369.
[25] Y. Wang, Z. Wang, Z. Wang, A stochastic load demand-oriented synergetic optimal control strategy for variable-speed pumps in residential district heating or cooling systems, Energy Build. 238 (2021) 110853.
[26] T. Zakula, P.R. Armstrong, L. Norford, Advanced cooling technology with thermally activated building surfaces and model predictive control, Energy Build. 86 (2015) 640–650.
[27] C. Zhang, M. Pomianowski, P.K. Heiselberg, et al., A review of integrated radiant heating/cooling with ventilation systems- Thermal comfort and indoor air quality, Energy Build. 223 (2020) 110094.
[28] P.R. Sampaio, R. Salvazet, P. Mandel, et al., Simulation and optimal control of heating and cooling systems: a case study of a commercial building, Energy Build. 246 (2021) 111102.
[29] X. Pang, C. Duarte, P. Haves, F. Chuang, Testing and demonstration of model predictive control applied to a radiant slab cooling system in a building test facility, Energy Build. 172 (2018) 432–441.
[30] J. Joe, P. Karava, X. Hou, Y. Xiao, J. Hu, A distributed approach to model-predictive control of radiant comfort delivery systems in office spaces with localized thermal environments, Energy Build. 175 (2018) 173–188.
[31] J. Joe, P. Karava, A model predictive control strategy to optimize the performance of radiant floor heating and cooling systems in office buildings, Appl. Energy 245 (2019) 65–77.
[32] D. Zhang, X. Huang, D. Gao, X. Cui, N. Cai, Experimental study on control performance comparison between model predictive control and proportion-integral-derivative control for radiant ceiling cooling integrated with underfloor ventilation system, Appl. Therm. Eng. 143 (2018) 130–136.
[33] D. Zhang, N. Cai, X. Cui, X. Xia, J. Shi, X. Huang, Experimental investigation on model predictive control of radiant floor cooling combined with underfloor ventilation system, Energy 176 (2019) 23–33.
[34] M. Schmelas, T. Feldmann, P. Wellnitz, E. Bollin, Adaptive predictive control of thermo-active building systems (TABS) based on a multiple regression algorithm: first practical test, Energy Build. 129 (2016) 367–377.
[35] G. Lymperopoulos, P. Ioannou, Building temperature regulation in a multi-zone HVAC system using distributed adaptive control, Energy Build. 215 (2020) 109825.
[36] Y.-b. Meng, T.-Y. Li, G.-H. Liu, et al., Real-time dynamic estimation of occupancy load and an air-conditioning predictive control method based on image information fusion, Build. Environ. 173 (2020) 106741.
[37] S. Qiu, Z. Li, Z. Li, et al., Model-free control method based on reinforcement learning for building cooling water systems: validation by measured data-based simulation, Energy Build. 218 (2020) 110055.
[38] M.A. Hassan, O. Abdelaziz, Best practices and recent advances in hydronic radiant cooling systems – Part II: simulation, control, and integration, Energy Build. 224 (2020) 110263.
[39] Y. Yao, D.K. Shekhar, State of the art review on model predictive control (MPC) in Heating Ventilation and Air-conditioning (HVAC) field, Build. Environ. 200 (2021) 107952.
[40] M. Gholamzadehmir, C. Del Pero, S. Buffa, et al., Adaptive-predictive control strategy for HVAC systems in smart buildings – A review, Sustainable Cities Society 63 (2020) 102480.
[41] R. Jing, J. Wang, N. Shah, et al., Emerging supply chain of utilising electrical vehicle retired batteries in distributed energy systems, Adv. Appl. Energy 1 (2021) 100002.
[42] ANSI/ASHRAE. ASHRAE Guideline 14: measurement of energy and demand savings; 2014.
[43] DOE US. M&V guidelines: measurement and verification for performance-based contracts - version 4.0. Fed Energy Manag Progr; 2015.
[44] Efficiency Valuation Organization. International performance measurement and verification protocol: concepts and options for determining energy and water savings, vol. I. Energy Proj Financ Resour 2012. doi:DOE/GO-102002-1554.
[45] M. Royapoor, T. Roskilly, Building model calibration using energy and environmental data, Energy Build. 94 (2015) 109–120.
[46] G. Mustafaraj, D. Marini, A. Costa, M. Keane, Model calibration for building energy efficiency simulation, Appl. Energy 130 (2014) 72–85.
[47] G. Ciulla, A. D'Amico, Building energy performance forecasting: a multiple linear regression approach, Appl. Energy 253 (2019) 113500.
[48] H. Tang, T. Zhang, X.H. Liu, et al., A novel approximate harmonic method for the dynamic cooling capacity prediction of radiant slab floors with time variable solar radiation, Energy Build. 223 (2020) 110117.
[49] Y. Guo, J. Wang, H. Chen, G. Li, J. Liu, C. Xu, R. Huang, Y. Huang, Machine learning-based thermal response time ahead energy demand prediction for building heating systems, Appl. Energy 221 (2018) 16–27.
[50] Gaussian Process Regression Models.1994-2021 The MathWorks MATLAB, Inc.
[51] H. Park, D.Y. Park, Comparative analysis on predictability of natural ventilation rate based on machine learning algorithms, Build. Environ. 195 (2021) 107744.
[52] K. Zhao, X.-H. Liu, Y. Jiang, Application of radiant floor cooling in large space buildings – A review, Renew. Sustain. Energy Rev. 55 (2016) 1083–1096.
[53] A. Koca, Z. Gemici, Y. Topacoglu, G. Cetin, R.C. Acet, B.B. Kanbur, Experimental investigation of heat transfer coefficients between hydronic radiant heated wall and room, Energy Build. 82 (2014) 211–221.
[54] T. Cholewa, M. Rosiński, Z. Spik, M.R. Dudzińska, A. Siuta-Olcha, On the heat transfer coefficients between heated/cooled radiant floor and room, Energy Build. 66 (2013) 599–606.
[55] L. Zhang, X.-H. Liu, Y. Jiang, Experimental evaluation of a suspended metal ceiling radiant panel with inclined fins, Energy Build. 62 (2013) 522–529.
[56] B. Ning, S. Schiavon, F.S. Bauman, A novel classification scheme for design and control of radiant system based on thermal response time, Energy Build. 137 (2017) 38–45.